

Supplementary Information

Iridium(III)-based minor groove binding complexes as DNA photocleavage agents

Stephen O. Aderinto,^a Torsten John,^{b,§} Abdulmujeeb Onawole,^c Raphael Peter Galleh,^d and Jim A. Thomas^{a*}

^a Department of Chemistry, University of Sheffield, Sheffield, S3 7HF, UK. E-mail: james.thomas@sheffield.ac.uk

^b Department of Biological Engineering, Massachusetts Institute of Technology, Cambridge, MA 02139, USA.

^c Institute for Molecular Bioscience, The University of Queensland, St. Lucia, QLD 4072, Australia.

^d School of Clinical Dentistry, University of Sheffield, Sheffield, S10 2TA, UK.

[§] Current address: Max Planck Institute for Polymer Research, Ackermannweg 10, 55128 Mainz, Germany.

1 Experimental studies

1.1 Synthesis and characterisation

Microwave reactions were performed in a modified Discover Microwave instrument. Reactions were carried out under a closed condition in either a 10 mL vial or a 50 mL round-bottom flask. All ¹H NMR spectra were recorded using a Bruker AM250 machine working in a Fourier transform mode. Mass spectra were recorded on a Kratos MS80 mass spectrometer working in positive ion mode with an *m*-nitrobenzyl alcohol matrix. All UV-Visible spectra were recorded on a thermos regulated Varian-Carey Bio-300 UV-Visible spectrometer, using quartz cells of 10 mm path length at 25 °C. Spectra were baseline corrected using Cary Win UV software. Luminescence spectra were recorded on a thermos regulated FluoroMax-4 spectrophotometer operating in luminescence wavelength scan mode at 25 °C. For preparative HPLC employed for the purification of the complexes, the following system was adopted: 2 x Varian ProStar 210 solvent delivery modules with Varian ProStar 320 UV-Vis detector equipped with a Water XBridge Prep C18 5 μm OBD 19 x 250 mm Column and a Varian ProStar 701 Fraction Collector and a Varian ProStar 410 Autosampler. HPLC grade-solvents employed were deionised and Millipore water (with some 0.1% trifluoroacetic acid/formic acid, solvent A) and MeCN (solvent B) were used. The flow rate was 17 mL min⁻¹ and the chromatogram was detected at 241 nm and 228 nm for [Ir(bpy)₂(qtpy)](CF₃SO₃)₃ and [Ir(phen)₂(qtpy)](CF₃SO₃)₃, respectively.

The ligand qtpy and the complexes [Ir(bpy)₂(CF₃SO₃)₂]CF₃SO₃ and [Ir(phen)₂(CF₃SO₃)₂]CF₃SO₃ were synthesized using reported methods.^{1,2}

[Ir(bpy)₂(qtpy)](CF₃SO₃)₃; [1](CF₃SO₃)₃. [Ir(bpy)₂(CF₃SO₃)₂]CF₃SO₃ (0.20 g, 0.210 mmol) and qtpy (0.24 g, 0.774 mmol) were suspended in ethanol (15 mL) in a 50 mL round-bottom flask and the mixture was well purged with Ar for about 30 minutes and allowed to stir and reflux under this condition. The reaction mixture, which was initially a faint yellowish suspension, became increasingly deeply yellow with the passage of time. After the complete dissolution of the reacting materials after about 2 days, the mixture was subjected to microwave irradiation for about 9 hours in a 50 mL round-bottom flask under a closed reflux condition. The desired complex was isolated by precipitating the reaction mixture with chilled Et₂O. Further precipitation of the complex was afforded by keeping the mixture cool at 0 °C in a

fridge. All portions were then reunited and dried *in vacuo*. Purification of the product was afforded by HPLC at a detection wavelength of 241 nm. A sample of the product was dissolved in MeCN and eluted through a column initially using 5% MeCN in water (0.1% TFA), which was increased over 20 minutes to 95% organic phase at the flow rate of 17 mL/min. The desired peak, which was eluted at 6.90 minutes as detected by UV-Vis spectroscopy, was collected and analysed. The yield of the crude product was calculated against $[\text{Ir}(\text{bpy})_2(\text{CF}_3\text{SO}_3)_2]\text{CF}_3\text{SO}_3$ with the characterisation data given below.

Yield: 0.24 g (88.89%). **ESI-MS, m/z:** 272 [M^{3+}]. **$^1\text{H NMR}$ (400 MHz, d^3 -(MeOD):** δ 9.87 (d, $J = 5.8$ Hz, 1H), 9.45 (d, $J = 4.7$ Hz, 1H), 8.73 (d, $J = 8.5$ Hz, 2H), 8.68 – 8.61 (m, 3H), 8.55 (d, $J = 10.8$ Hz, 5H), 8.32 (s, 2H), 8.15 (t, $J = 7.1$ Hz, 1H), 8.09 – 8.03 (m, 2H), 7.96 (d, $J = 6.6$ Hz, 1H), 7.86 (dd, $J = 23.0$, 16.9 Hz, 4H), 7.55 (s, 1H), 7.36 (d, $J = 5.9$ Hz, 1H).

$[\text{Ir}(\text{phen})_2(\text{qtpy})](\text{CF}_3\text{SO}_3)_3$; **[2](CF_3SO_3) $_3$. $[\text{Ir}(\text{phen})_2(\text{CF}_3\text{SO}_3)_2]\text{CF}_3\text{SO}_3$ (0.2 g, 0.196 mmol) and qtpy (0.20 g, 0.646 mmol) were suspended in EtOH (35 mL) in a 50 mL round-bottom flask and the mixture was well purged with Ar for about 30 minutes and allowed to stir and reflux under this condition. The reaction mixture, which was initially a faint yellowish suspension, became increasingly deeply yellow with the passage of time. Complete dissolution of the reacting materials was attained at about 1 hour whilst the mixture was allowed to further reflux for about 1–2 days. After the complete dissolution of the reacting materials at about 2 days, the mixture was then subjected to microwave irradiation for about 9 hours in a 50 mL round-bottom flask under a closed reflux condition. The desired complex was isolated by precipitating the reaction mixture with chilled Et₂O. Further precipitation of the complex was afforded by keeping the mixture cool at 0 °C in a fridge. All portions were then reunited and dried *in vacuo*. Purification of the product was afforded by HPLC at a detection wavelength of 228 nm. A sample of the product was dissolved in MeCN and eluted through a column initially using 5% MeCN in water (0.1% TFA), which was increased over 20 minutes to 95% organic phase at the flow rate of 17 mL/min. The desired peak, which was eluted at 8.16 minutes as detected by UV-Vis spectroscopy, was collected and analysed. The yield of the crude product was calculated against $[\text{Ir}(\text{phen})_2(\text{CF}_3\text{SO}_3)_2]\text{CF}_3\text{SO}_3$ with the characterisation data given below:**

Yield: 0.17g (50%). **ESI-MS, m/z:** 506 [M^{2+}], 287 [M^{3+}]. **$^1\text{H NMR}$ (400 MHz, d^3 -(acetone) δ_{H} :** 10.30 (d, 2H), 10.18 (dt, $J = 11.1$, 6.3 Hz, 2H), 10.05 (dd, $J = 9.8$, 5.1 Hz, 2H), 9.74 (d, $J = 5.4$ Hz, 2H), 9.40 – 9.16 (m, 2H), 8.93 (t, $J = 8.9$ Hz, 2H), 8.86 – 8.73 (m, 2H), 8.71 – 8.37 (m, 4H), 8.27 – 8.20 (dd, 4H), 8.16 (d, $J = 5.4$ Hz, 2H), 8.03 (d, $J = 5.5$ Hz, 2H), 7.96 – 7.84 (m, 2H), 7.76 (m, $J = 25.2$, 8.4, 5.5 Hz, 4H).

1.2 Supporting experimental results

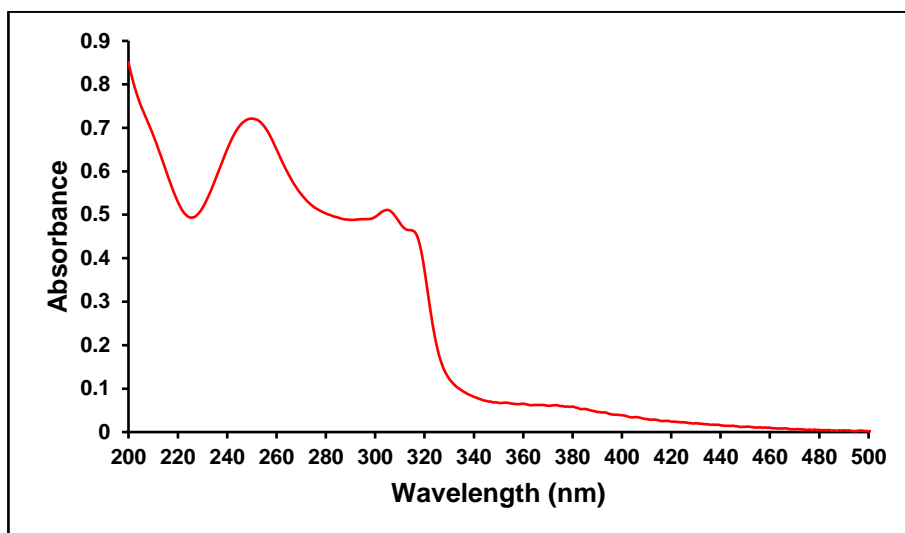


Figure S1. UV-Vis spectrum of 29.60 μM $[\text{Ir}(\text{bpy})_2(\text{qtpy})]\text{Cl}_3$ in tris buffer.

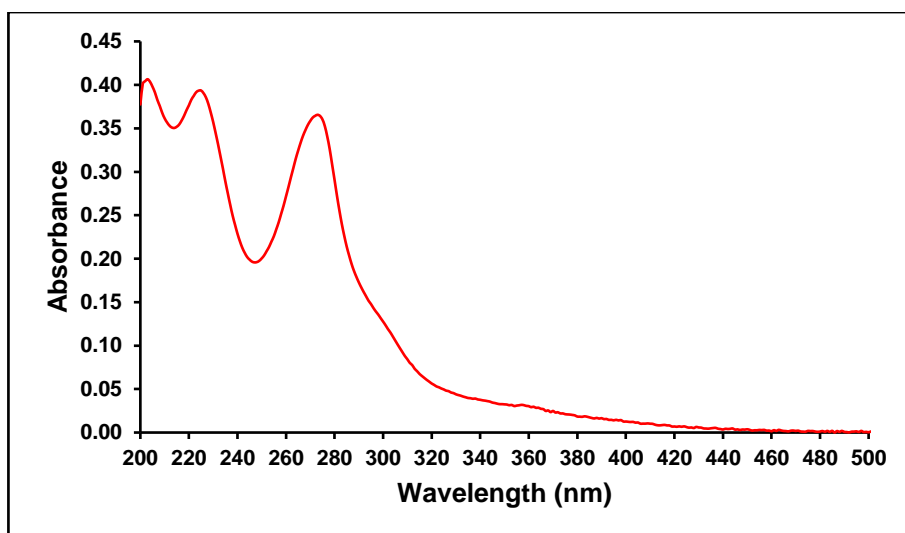


Figure S2. UV-Vis spectrum of 8.37 μM $[\text{Ir}(\text{phen})_2(\text{qtpy})]\text{Cl}_3$ in tris buffer.

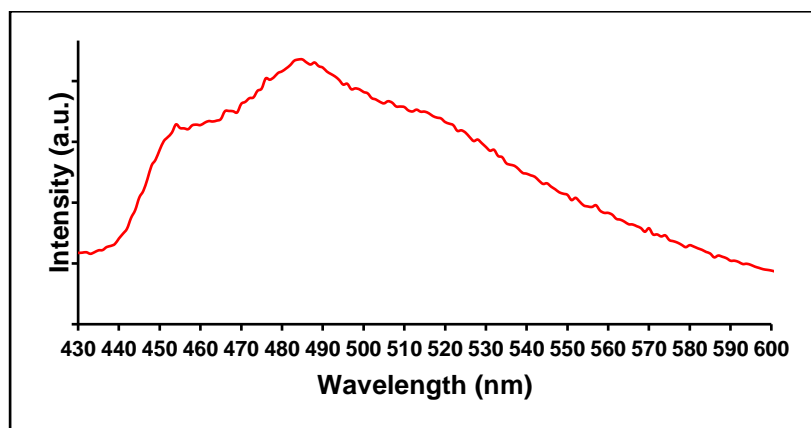


Figure S3. Emission spectrum of $[\text{Ir}(\text{bpy})_2(\text{qtpy})]\text{Cl}_3$ in tris buffer.

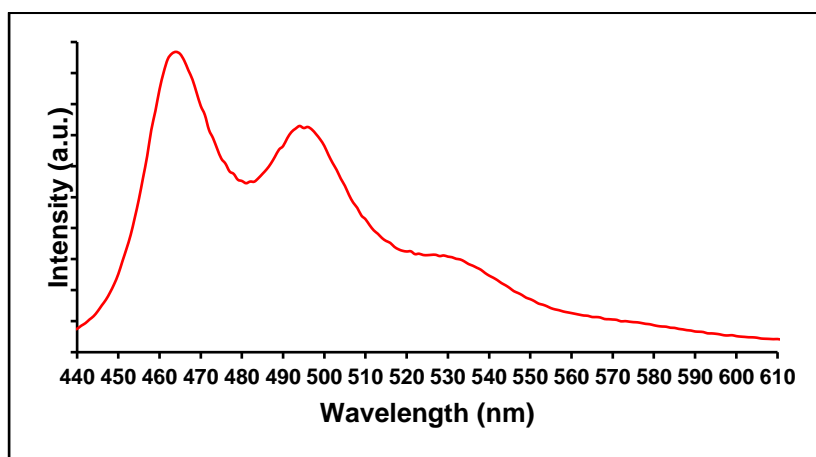


Figure S4. Emission spectrum of $8.37 \mu\text{M}$ $[\text{Ir}(\text{phen})_2(\text{qtpy})]\text{Cl}_3$ in tris buffer.

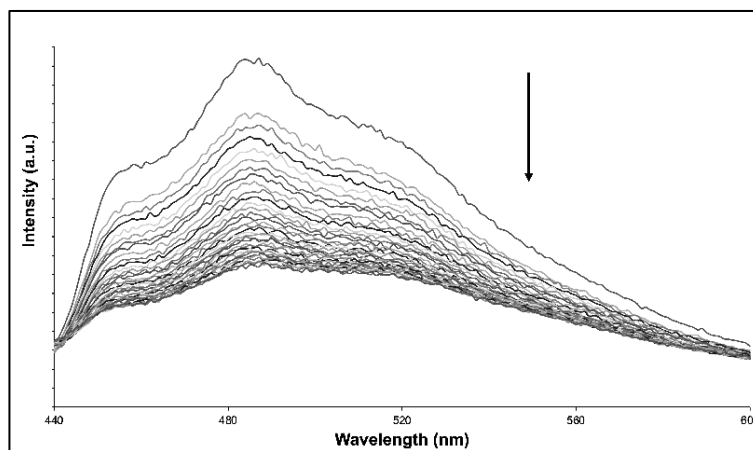


Figure S5. Luminescent titration of 16 mM thymus-DNA, CT-DNA, into a solution of $100 \mu\text{M}$ of **1** in 5 mM tris buffer, 25 mM NaCl, pH 7.4, at $27 \text{ }^\circ\text{C}$.

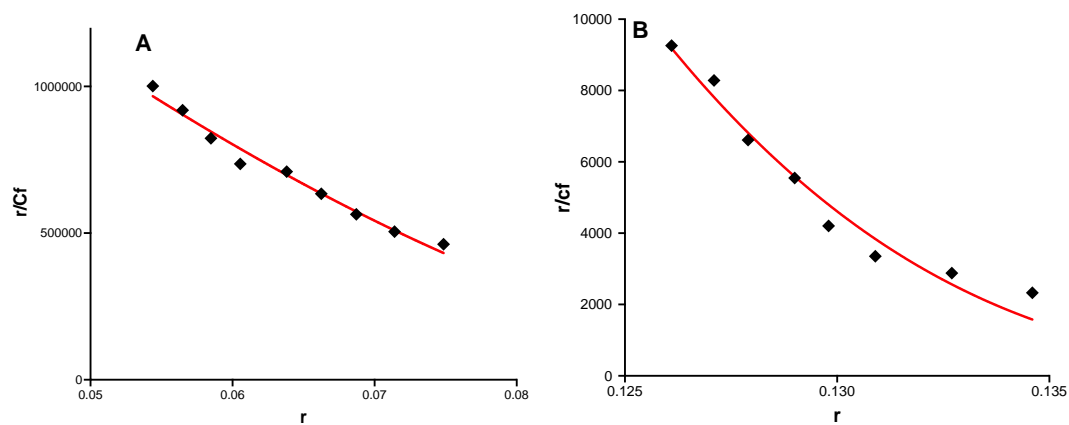


Figure S6. Scatchard Plots for the interaction of Complex **1** (A) and Complex **2** (B) with duplex DNA with fit to McGhee-von Hippel model (shown as continuous red line) that gave the parameters discussed in the main report. Fits were obtained using GraphPad Prism 10.

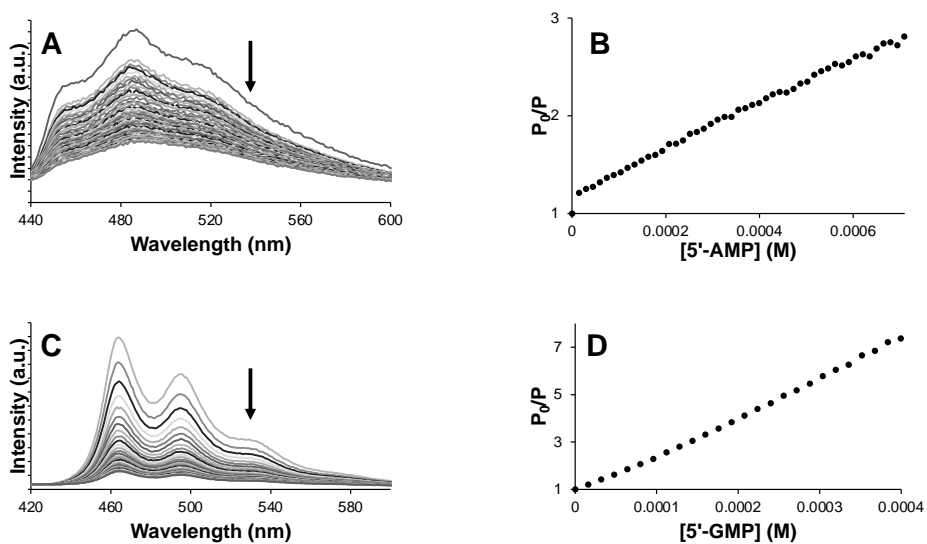


Figure S7. Quenching of luminescence of complexes by nucleotides. (A) Change in emission from an aqueous solution of **1** upon successive addition of 5'-AMP. (B) Stern-Volmer plot derived from data shown in A. (C) Change in emission from an aqueous solution of **2** upon successive addition of 5'-GMP (D) Stern-Volmer plot derived from data shown in C.

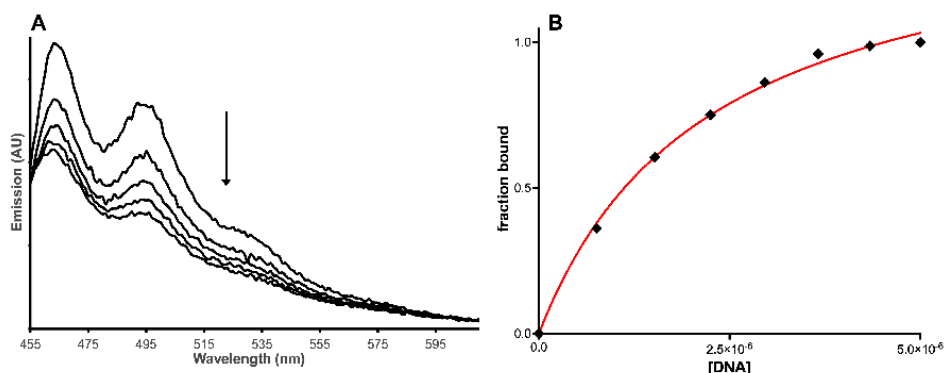


Figure S8. (A) Luminescence response induced through progressive addition of 0.85 μM of quadruplex folded HTS to Complex **2**. (B) Binding curve for **2** with HTS constructed using emission data – continuous red line shows fitting to binding to one-set-of-sites that gave the parameters discussed in the main report.

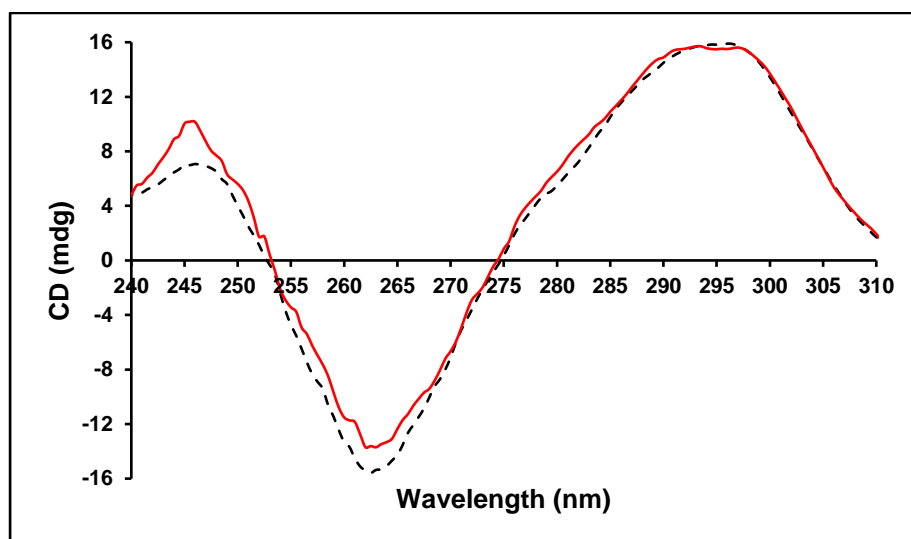


Figure S9. CD spectrum of 5.65 μM HTS (G4 oligonucleotide sequence) (black broken line) and in the presence of a solution of 31.50 μM of **1** (red line) in PBS buffer, pH 7.41 at 25°C.

2 Density functional theory (DFT) calculations

2.1 DFT method

DFT was used to calculate optimised structures, electrostatic potentials, and frontier orbitals. The Gaussian 09 programme was employed for these DFT calculations.³ The Becke-three-parameters Lee-Yang and Parr (B3LYP) basis set^{4,5} was used whilst the 6-31g(d) basis⁶ was applied to all atoms except for iridium in which the LANL2DZ (Los Alamos National Laboratory 2 Double-Zeta) was applied.⁷⁻¹⁰ This method of mixing two different basis set was used to reduce the computational cost involved in the calculation.^{11,12} An effective core potential (ECP) basis set (LANL2DZ) was applied for the transition metal to implicitly account for scalar relativistic effects.^{13,14} The stability of the optimized geometries of the studied complexes was confirmed via frequency calculations which showed the absence of imaginary frequencies. TDDFT (Time Dependent-Density Functional Theory) calculations¹⁵ were

utilised to calculate optical transitions (UV-Vis) using the same level of theory on 100 states set in acetonitrile as the solvent via the Self-Consistent Reaction Field (SCRF).¹⁶

2.2 Supporting DFT results

Table S1. Selected bond lengths from the DFT optimised geometries.

	Complex 1	Complex 2
Bond	Length (Å)	
Ir–N ₂	2.089	2.102
Ir–N ₃	2.079	2.089
Ir–N ₄	2.083	2.081
Ir–N ₅	2.089	2.080
Ir–N ₆	2.092	2.097
Ir–N ₇	2.094	2.101

3 Molecular dynamics (MD) simulations

3.1 Structures and force field parameterisation for iridium(III) complexes

Geometry optimised structures of the Ir(III)-polypyridine complexes were obtained from DFT calculations. Since transition metal complexes are not well described in typical MD force fields, the complexes had to be parameterised. The AmberTools21¹⁷ program antechamber¹⁸ was used to assign atom types for the ligands using the Generalized Amber Force Field (GAFF).¹⁹ The tool parmchk2 was applied to assign missing angle and dihedral parameters. We used the MCPB.py tool, a python based metal center parameter builder (MCPB),^{20,21} implemented in AmberTools21,¹⁷ to determine force field parameters for the Ir(III)-polypyridine complexes. This tool uses a small and a large model to balance accuracy and speed for the parameterisation of metal-containing systems. The small model is used to describe the metal associated bond and angle parameters, while the large model is used to describe the partial charges of the entire system.²⁰ MCPB.py prepares the input files for quantum mechanical (QM) calculations, in our case, for Gaussian 16 (Revision C01).³ DFT calculations were performed using the B3LYP^{5,22} level of theory with the 6-31G* basis set⁶ for the ligands, while the LANL2 effective core potential (ECP) with double zeta (DZ) valence basis set (LANL2DZ),⁷⁻¹⁰ a pseudo-potential, was applied for iridium (charge: +3, multiplicity: 1). This approach of using ECPs is common for transition metals to reduce computational cost. Following geometry optimisation of the small model, the Seminario method was used to generate the force constants for bond and angle parameters by evaluation of the Cartesian Hessian matrix.²³ RESP charge fitting was performed for the large model with the charges of the heavy backbone atoms fixed to values from the AMBER force field, except for the ligand atoms bound to the metal centre. The Ir³⁺ van der Waals (VDW) radius was set to 1.42 Å during the Merz-Kollman population analysis, adapted by the MCPB.py tool from the universal force field (UFF).²⁴ MCPB.py finally generated a PDB file with renamed metal site residues and leap input for AMBER for a bonded model. The atom types and charges for complexes 1 and 2 are presented in Tables S2 and S3 respectively.

Force field parameters (bonds, angles, dihedrals) are provided in the zipped folder 'Force-Field-Parameters-Ir-Complexes.zip' as SI.

Table S2. Atom types and charges for complex 1 / [Ir(bpy)₂(qtpy)]³⁺.

Atom	Type	Charge	Atom	Type	Charge	Atom	Type	Charge
IR	M1	-0.135581	C13	ca	-0.032088	H20	h4	0.107382
N1	Y1	0.060758	H10	ha	0.182343	N6	nb	-0.399169
N2	Y2	0.029811	C14	ca	-0.07534	C30	ca	0.243163
N3	Y3	0.038607	H11	ha	0.175237	H21	h4	0.09019
N4	Y4	0.058397	C15	ca	-0.045892	C31	ca	-0.161795
N5	Y5	0.054541	H12	h4	0.132784	H22	ha	0.10252
C1	cp	0.072621	C16	ca	-0.106928	C32	ca	-0.15126
C2	ca	-0.103959	H13	h4	0.144523	H23	ha	0.100759
H1	ha	0.165437	C17	ca	-0.049594	C33	ca	0.24411
C3	ca	-0.032249	H14	ha	0.156174	H24	h4	0.094037
H2	ha	0.182722	C18	cp	0.073742	N7	nb	-0.408207
C4	ca	-0.075374	C19	ca	-0.064521	C34	ca	0.243737
H3	ha	0.175309	H15	ha	0.136754	H25	h4	0.093726
C5	ca	-0.048706	C20	cp	0.035019	C35	ca	-0.179834
H4	h4	0.135382	C21	cp	0.034575	H26	ha	0.107587
C6	ca	-0.051986	C22	ca	-0.054071	N	Y6	0.050507
H5	h4	0.133438	H16	ha	0.125397	C36	ca	-0.029496
C7	ca	-0.072749	C23	cp	0.05877	H27	ha	0.181187
H6	ha	0.17508	C24	ca	-0.050243	C37	cp	0.050977
C8	ca	-0.027806	H17	ha	0.154817	C38	ca	-0.053573
H7	ha	0.180753	C25	ca	-0.103584	H28	h4	0.132668
C9	ca	-0.098228	H18	h4	0.145939	C39	ca	-0.069454
H8	ha	0.164016	C26	cp	0.029326	H29	ha	0.174203
C10	cp	0.046654	C27	cp	0.043968	C	ca	-0.097346
C11	cp	0.076671	C28	ca	-0.154127	H	ha	0.16271
C12	ca	-0.106179	H19	ha	0.107357			
H9	ha	0.164244	C29	ca	0.208704			

Table S3. Atom types and charges for complex 2 / [Ir(phen)₂(qtpy)]³⁺.

Atom	Type	Charge	Atom	Type	Charge	Atom	Type	Charge
IR	M1	-0.152502	H9	ha	0.173559	C32	cp	0.065922
N1	Y1	-0.005643	C14	ca	0.079898	C33	ca	-0.184535
N2	Y2	0.012146	C15	ca	0.081174	H19	ha	0.099464
N3	Y3	0.079029	C16	ca	0.08322	C34	ca	0.262781
N4	Y4	0.079035	C17	ca	0.069797	H20	h4	0.086301
N5	Y5	0.012178	C18	ca	-0.043673	N7	nb	-0.423329
N6	Y6	-0.005633	H10	ha	0.172365	C35	ca	0.268934
C1	ca	-0.034338	C19	ca	-0.1058	H21	h4	0.087178
H1	h4	0.143353	H11	ha	0.177473	C36	ca	-0.193524
C2	ca	-0.100643	C20	ca	-0.036708	H22	ha	0.108853
H2	ha	0.177262	H12	h4	0.145412	C37	ca	-0.193645
C3	ca	-0.051214	C21	ca	-0.125456	H23	ha	0.108887
H3	ha	0.173556	H13	h4	0.153227	C38	ca	0.26916
C4	ca	0.079839	C22	ca	-0.052515	H24	h4	0.087139
C5	ca	0.081196	H14	ha	0.15543	N	nb	-0.423424
C6	ca	0.083285	C23	cp	0.069084	C39	ca	0.262777
C7	ca	0.069716	C24	ca	-0.066844	H25	h4	0.086316
C8	ca	-0.043727	H15	ha	0.135471	C40	ca	-0.184547
H4	ha	0.172386	C25	cp	0.021972	H26	ha	0.099475
C9	ca	-0.105816	C26	cp	0.02196	C41	ca	-0.141288
H5	ha	0.177622	C27	ca	-0.066833	H27	ha	0.185583
C10	ca	-0.036839	H16	ha	0.135475	C42	ca	-0.137765
H6	h4	0.145395	C28	cp	0.069055	H28	ha	0.184715
C11	ca	-0.03432	C29	ca	-0.052507	C43	ca	-0.141338
H7	h4	0.143339	H17	ha	0.155439	H29	ha	0.185562
C12	ca	-0.100651	C30	ca	-0.125476	C	ca	-0.137749
H8	ha	0.177264	H18	h4	0.153245	H	ha	0.184712
C13	ca	-0.051245	C31	cp	0.065907			

3.2 Structures and force field for DNA duplex and G-quadruplex

The CT-DNA used in experiments was modelled by a DNA duplex (B-form, sequence: AATTGGCCAATTGGCCAATT), generated using the nucleic acid builder (nab)²⁵ as implemented in AmberTools22.²⁶ For the G-quadruplex (22-nt human telomeric DNA, d[AGGG-(TTAGGG)₃]), the DNA structure was obtained from the Protein Data Bank (PDB entry: 143D).²⁷ The OL15 force field was used for the DNA,^{28–30} following the Cornell *et al.* force field family (FF99, BSC0).^{31–33}

3.3 Simulation setups and parameters


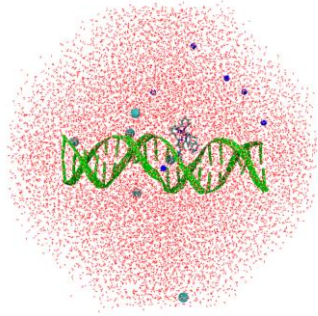
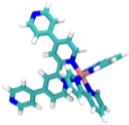
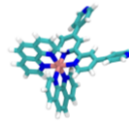
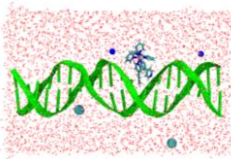
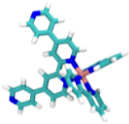
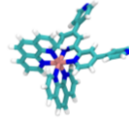
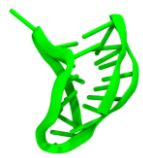
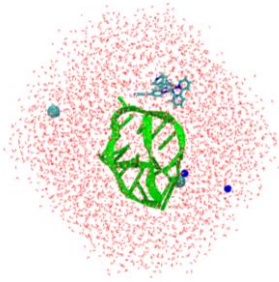
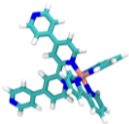
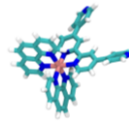
Initial simulation set-ups with the DNA duplex or G-quadruplex and the Ir(III)-complexes **1** and **2** in close proximity were prepared in BIOVIA Discovery Studio Visualizer v21.1.0 (Dassault Systèmes, Vélizy-Villacoublay, France). The AmberTools22²⁶ program tleap was used to prepare the simulation files by loading the structures and force field parameters, and solvating the systems with TIP3P water.³⁴ NaCl was used to electroneutralise the systems and add 25 mM of NaCl to reflect experimental conditions

(Joung-Cheatham parameters).³⁵ The DNA and Ir(III)-complex were placed in a truncated octahedral simulation box with 10 Å distance to the box edges. In addition, a separate set of simulations with the duplex in a rectangular box with 10 Å distance to the sides perpendicular to the duplex axis and 0 Å distance along the duplex axis were prepared to model an infinite long duplex and reflect experimentally used CT-DNA.

Large scale MD simulations were performed in Amber and AmberTools 22^{26,36,37} on the MIT SuperCloud³⁸ with the support of the CUDA version^{39–41} of Amber on NVIDIA V100 GPUs. DNA was described using the OL15 force field^{28–30} and Ir(III) complexes using the GAFF force field,¹⁹ as ascribed above. Periodic boundary conditions (PBC) were applied. Electrostatic interactions were computed using the Particle Mesh Ewald (PME) method with a grid spacing of about 0.1 nm (NFFT1-3 values were approximately equal to the box dimensions).⁴² A cutoff of 1.2 nm was used to calculate nonbonded interactions. Bonds involving hydrogen were constrained to their equilibrium values using SHAKE.⁴³

Prior to starting the MD simulations, each system was first energy minimised with the DNA and Ir(III)-complexes position-restrained ($500 \text{ kcal mol}^{-1} \text{ \AA}^{-2}$) using the steepest descent algorithm (2000 steps) and conjugate gradient algorithm (3000 steps), followed by the same steps without position restraints applied. A time step of 2 fs was used for the MD simulations. MD simulations were started with an initial equilibration by heating the systems from 0 K to 300 K with weak position restraints applied to DNA and Ir(III)-complexes ($10 \text{ kcal mol}^{-1} \text{ \AA}^{-2}$) for 20 ps, followed by a 200 ps simulation in a NPT ensemble at 300 K and 1 bar without restraints. The temperature was stabilized using Langevin dynamics⁴⁴ with a collision frequency of 5 ps^{-1} and the pressure was stabilized using the Berendsen barostat⁴⁵ with isotropic position scaling with a relaxation time of 2 ps. Production MD simulations were run for 500 ns in triplicate with random starting velocities (see Table S4 for an overview of simulation setups).

Table S4. Overview of MD simulations.

DNA Structure	Box Type	Ir(III)-Complex	Simulations
Duplex, B-form d[AATTGGCCAATTGGCCAATT] 	truncated octahedron with 10 Å distance between the solute and the box edges 	1 / [Ir(bpy) ₂ (qtpy)] ³⁺ 	3 x 500 ns
		2 / [Ir(phen) ₂ (qtpy)] ³⁺ 	3 x 500 ns
	Rectangular box with 10 Å distance to the sides perpendicular to the DNA duplex axis and 0 Å distance along the duplex axis 	1 / [Ir(bpy) ₂ (qtpy)] ³⁺ 	3 x 500 ns
		2 / [Ir(phen) ₂ (qtpy)] ³⁺ 	3 x 500 ns
G-Quadruplex d[AGGG-(TTAGGG) ₃] 	truncated octahedron with 10 Å distance between the solute and the box edges 	1 / [Ir(bpy) ₂ (qtpy)] ³⁺ 	3 x 500 ns
		2 / [Ir(phen) ₂ (qtpy)] ³⁺ 	3 x 500 ns

3.4 Simulation Analysis

MD simulations were analysed using the AmberTools 22 program CPPTRAJ.⁴⁶ VMD software was used for visualization of trajectories.⁴⁷ To identify the most dominant binding motifs of the Ir(III)-complexes to the DNA structures, clustering of the simulation trajectories was performed over all repetitions for each system (hierarchical agglomerative clustering algorithm, average linkage, 5-12 clusters each). The solvent accessible surface area (SASA) of the Ir(III)-complexes was calculated using the LCPO algorithm by Weiser *et al.*⁴⁸

3.5 Supporting MD results

3.5.1 Representative Structures

The most dominant Ir(III)-complex binding motifs to a DNA duplex and the G-quadruplex were determined from analysing the trajectories and clustering them based on their similarity. The most central structure of the largest clusters are shown in Figures S10 and S11.

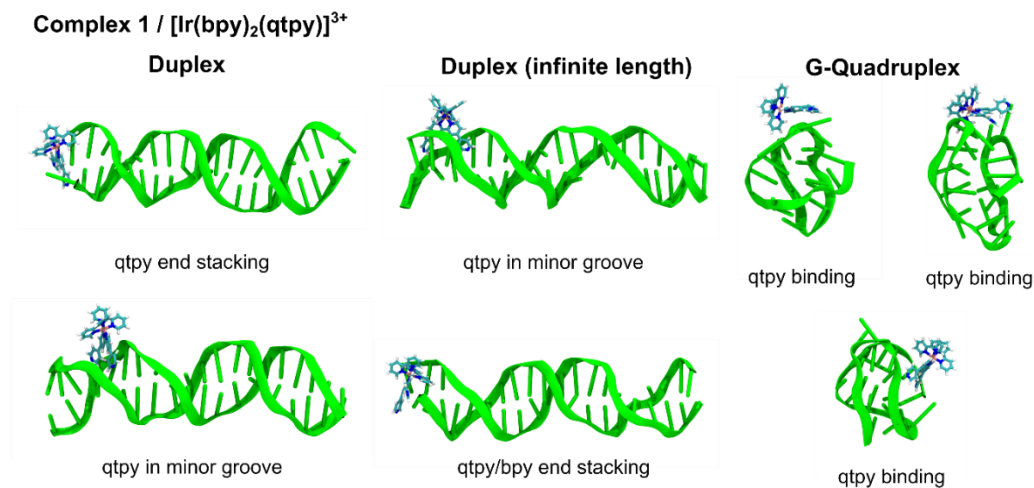


Figure S10. Most dominant binding motifs of complex 1 to DNA duplex and G-quadruplex in MD simulations. The qtpy ligand either bound to the duplex minor groove or stacked to the duplex ends. Binding to the G-quadruplex was more flexible.

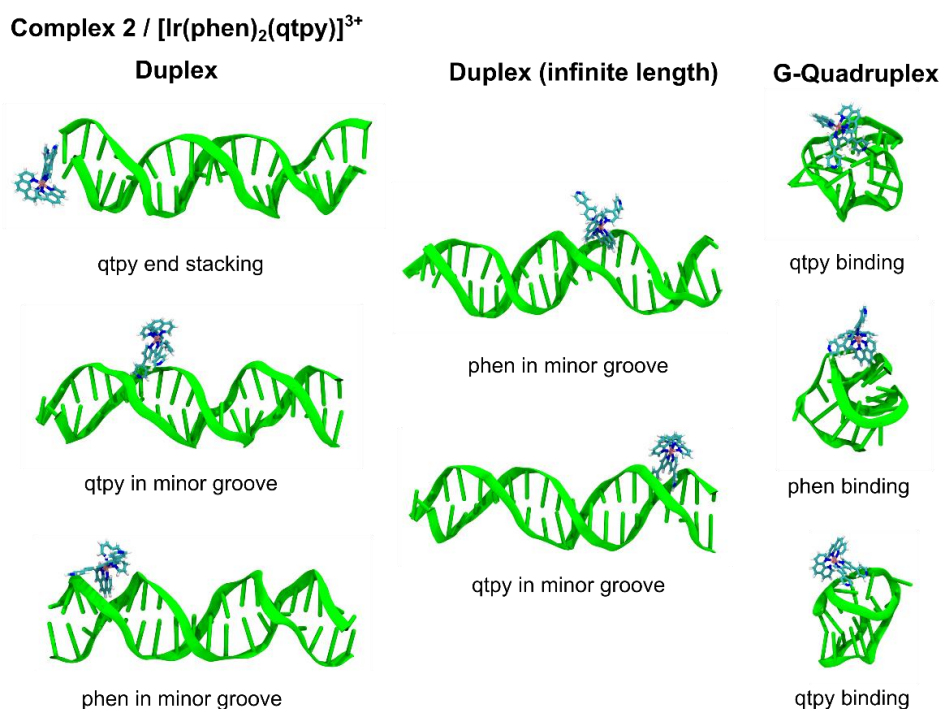


Figure S11. Most dominant binding motifs of complex 2 to DNA duplex and G-quadruplex in MD simulations. The qtpy and phen ligands mostly bound to the duplex minor groove, while stacking at the duplex end was also observed. Binding to the G-quadruplex was more flexible.

Supporting references

- 1 K. Bierig, R. J. Morgan, S. Tysoe, H. D. Gafney, T. C. Streakas and A. D. Baker, *Inorg. Chem.*, 1991, **30**, 4898–4903.
- 2 M. Pandrala, F. Li, L. Wallace, P. J. Steel, B. Moore II, J. Autschbach, J. G. Collins and F. R. Keene, *Aust. J. Chem.*, 2013, **66**, 1065–1073.
- 3 M. J. Frisch, G. W. Trucks, H. B. Schlegel, G. E. Scuseria, M. A. Robb, J. R. Cheeseman, G. Scalmani, V. Barone, G. A. Petersson, H. Nakatsuji, X. Li, M. Caricato, A. Marenich, J. Bloino, B. G. Janesko, R. Gomperts, B. Mennucci, H. P. Hratchian, J. V. Ortiz, A. F. Izmaylov, J. L. Sonnenberg, D. Williams-Young, F. Ding, F. Lipparini, F. Egidi, J. Goings, B. Peng, A. Petrone, T. Henderson, D. Ranasinghe, V. G. Zakrzewski, J. Gao, N. Rega, G. Zheng, W. Liang, M. Hada, M. Ehara, K. Toyota, R. Fukuda, J. Hasegawa, M. Ishida, T. Nakajima, Y. Honda, O. Kitao, H. Nakai, T. Vreven, K. Throssell, J. A. Montgomery, Jr., J. E. Peralta, F. Ogliaro, M. Bearpark, J. J. Heyd, E. Brothers, K. N. Kudin, V. N. Staroverov, T. Keith, R. Kobayashi, J. Normand, K. Raghavachari, A. Rendell, J. C. Burant, S. S. Iyengar, J. Tomasi, M. Cossi, J. M. Millam, M. Klene, C. Adamo, R. Cammi, J. W. Ochterski, R. L. Martin, K. Morokuma, O. Farkas, J. B. Foresman, and D. J. Fox, Gaussian 09, Revis. A.02, and Gaussian 16, Revis. C.01, 2016, Wallingford CT.
- 4 A. D. Becke, *J. Chem. Phys.*, 1993, **98**, 1372–1377.
- 5 P. J. Stephens, F. J. Devlin, C. F. Chabalowski and M. J. Frisch, *J. Phys. Chem.*, 1994, **98**, 11623–11627.
- 6 W. J. Hehre, R. Ditchfield and J. A. Pople, *J. Chem. Phys.*, 1972, **56**, 2257–2261.
- 7 T. H. Dunning Jr. and P. J. Hay, in *Methods of Electronic Structure Theory*, Plenum Press, 2nd edn., 1977, pp. 1–27.
- 8 W. R. Wadt and P. J. Hay, *J. Chem. Phys.*, 1985, **82**, 284–298.
- 9 P. J. Hay and W. R. Wadt, *J. Chem. Phys.*, 1985, **82**, 270–283.
- 10 P. J. Hay and W. R. Wadt, *J. Chem. Phys.*, 1985, **82**, 299–310.
- 11 Y. Yang, M. N. Weaver and K. M. Merz, *J. Phys. Chem. A*, 2009, **113**, 9843–9851.
- 12 M. X. Song, G. Q. Xi, H. Y. Chi, K. C. He, L. U. Peng, Z. K. Qin, Y. L. Zhang, L. U. Shi-Quan and H. J. Zhang, *Appl. Organomet. Chem.*, 2020, **34**, 1–9.
- 13 B. Liu, S. Monro, Z. Li, M. A. Javed, D. Ramirez, C. G. Cameron, K. Colón, J. Roque, S. Kilina, J. Tian, S. A. Mcfarland and W. Sun, *ACS Appl. Bio Mater.*, 2019, **2**, 2964–2977.
- 14 S. S. Bhat, N. Shivalingegowda, V. K. Revankar, N. K. Lokanath, M. S. Kugaji, V. Kumbar and K. Bhat, *J. Inorg. Biochem.*, 2017, **177**, 127–137.
- 15 M. E. Casida, C. Jamorski, K. C. Casida and D. R. Salahub, *J. Chem. Phys.*, 1998, **108**, 4439–4449.
- 16 M. Cossi, V. Barone, B. Mennucci and J. Tomasi, *Chem. Phys. Lett.*, 1998, **286**, 253–260.
- 17 D. A. Case, H. M. Aktulga, K. Belfon, I. Y. Ben-Shalom, S. R. Brozell, D. S. Cerutti, T. E. Cheatham III, G. A. Cisneros, V. W. D. Cruzeiro, T. A. Darden, R. E. Duke, G. Giambasu, M. K. Gilson, H. Gohlke, A. W. Goetz, R. Harris, S. Izadi, S. A. Izmailov, C. Jin, K. Kasavajhala, M. C. Kaymak, E. King, A. Kovalenko, T. Kurtzman, T. S. Lee, S. LeGrand, P. Li, C. Lin, J. Liu, T. Luchko, R. Luo, M. Machado, V. Man, M. Manathunga, K. M. Merz, Y. Miao, O. Mikhailovskii, G. Monard, H. Nguyen, K. A. O’Hearn, A. Onufriev, F. Pan, S. Pantano, R. Qi, A. Rahnamoun, D. R. Roe, A. Roitberg, C. Sagui, S. Schott-Verdugo, J. Shen, C. L. Simmerling, N. R. Skrynnikov, J. Smith, J. Swails, R. C. Walker, J. Wang, H. Wei, R. M. Wolf, X. Wu, Y. Xue, D. M. York, S. Zhao and P. A. Kollman, *AmberTools21*, 2021, University of California, San Francisco.
- 18 J. Wang, W. Wang, P. A. Kollman and D. A. Case, *J. Mol. Graph. Model.*, 2006, **25**, 247–260.
- 19 J. Wang, R. M. Wolf, J. W. Caldwell, P. A. Kollman and D. A. Case, *J. Comput. Chem.*, 2004, **25**, 1157–1174.
- 20 P. Li and K. M. Merz, *J. Chem. Inf. Model.*, 2016, **56**, 599–604.
- 21 P. Li and K. M. Merz Jr., in *Springer Protocols, Structural Genomics General Applications*, eds. Y. W. Chen and C.-P. B. Yiu, Springer US, New York, NY, 2021, vol. 2199, pp. 257–275.

- 22 A. D. Becke, *J. Chem. Phys.*, 1993, **98**, 5648–5652.
- 23 J. M. Seminario, *Int. J. Quantum Chem.*, 1996, **60**, 1271–1277.
- 24 A. K. Rappé, C. J. Casewit, K. S. Colwell, W. A. Goddard and W. M. Skiff, *J. Am. Chem. Soc.*, 1992, **114**, 10024–10035.
- 25 T. J. Macke and D. A. Case, in *ACS Symposium Series*, 1998, vol. 682, pp. 379–393.
- 26 D. A. Case, H. M. Aktulga, K. Belfon, I. Y. Ben-Shalom, J. T. Berryman, S. R. Brozell, D. S. Cerutti, T. E. Cheatham III, G. A. Cisneros, V. W. D. Cruzeiro, T. A. Darden, R. E. Duke, G. Giambasu, M. K. Gilson, H. Gohlke, A. W. Goetz, R. Harris, S. Izadi, S. A. Izmailov, K. Kasavajhala, M. C. Kaymak, E. King, A. Kovalenko, T. Kurtzman, T. S. Lee, S. LeGrand, P. Li, C. Lin, J. Liu, T. Luchko, R. Luo, M. Machado, V. Man, M. Manathunga, K. M. Merz, Y. Miao, O. Mikhailovskii, G. Monard, H. Nguyen, K. A. O’Hearn, A. Onufriev, F. Pan, S. Pantano, R. Qi, A. Rahnamoun, D. R. Roe, A. Roitberg, C. Sagui, S. Schott-Verdugo, A. Shajan, J. Shen, C. L. Simmerling, N. R. Skrynnikov, J. Smith, J. Swails, R. C. Walker, J. Wang, J. Wang, H. Wei, R. M. Wolf, X. Wu, Y. Xiong, Y. Xue, D. M. York, S. Zhao and P. A. Kollman, *Amber22 and AmberTools22*, 2022, University of California, San Francisco.
- 27 Y. Y. Wang and D. J. D. J. Patel, *Structure*, 1993, **1**, 263–282.
- 28 M. Zgarbová, J. Šponer, M. Otyepka, T. E. Cheatham, R. Galindo-Murillo and P. Jurečka, *J. Chem. Theory Comput.*, 2015, **11**, 5723–5736.
- 29 M. Zgarbová, F. J. Luque, J. Šponer, T. E. Cheatham, M. Otyepka and P. Jurečka, *J. Chem. Theory Comput.*, 2013, **9**, 2339–2354.
- 30 M. Krepl, M. Zgarbová, P. Stadlbauer, M. Otyepka, P. Banáš, J. Koča, T. E. Cheatham, P. Jurečka and J. Šponer, *J. Chem. Theory Comput.*, 2012, **8**, 2506–2520.
- 31 W. D. Cornell, P. Cieplak, C. I. Bayly, I. R. Gould, K. M. Merz, D. M. Ferguson, D. C. Spellmeyer, T. Fox, J. W. Caldwell and P. A. Kollman, *J. Am. Chem. Soc.*, 1995, **117**, 5179–5197.
- 32 J. Wang, P. Cieplak and P. A. Kollman, *J. Comput. Chem.*, 2000, **21**, 1049–1074.
- 33 A. Pérez, I. Marchán, D. Svozil, J. Sponer, T. E. Cheatham, C. A. Loughton and M. Orozco, *Biophys. J.*, 2007, **92**, 3817–3829.
- 34 W. L. Jorgensen, J. Chandrasekhar, J. D. Madura, R. W. Impey and M. L. Klein, *J. Chem. Phys.*, 1983, **79**, 926–935.
- 35 I. S. Joung and T. E. Cheatham, *J. Phys. Chem. B*, 2008, **112**, 9020–9041.
- 36 R. Salomon-Ferrer, D. A. Case and R. C. Walker, *Wiley Interdiscip. Rev. Comput. Mol. Sci.*, 2013, **3**, 198–210.
- 37 D. A. Case, T. E. Cheatham, T. Darden, H. Gohlke, R. Luo, K. M. Merz, A. Onufriev, C. Simmerling, B. Wang and R. J. Woods, *J. Comput. Chem.*, 2005, **26**, 1668–1688.
- 38 A. Reuther, J. Kepner, C. Byun, S. Samsi, W. Arcand, D. Bestor, B. Bergeron, V. Gadepally, M. Houle, M. Hubbell, M. Jones, A. Klein, L. Milechin, J. Mullen, A. Prout, A. Rosa, C. Yee and P. Michaleas, in *2018 IEEE High Performance Extreme Computing Conference, HPEC 2018*, IEEE, 2018, pp. 1–6.
- 39 R. Salomon-Ferrer, A. W. Götz, D. Poole, S. Le Grand and R. C. Walker, *J. Chem. Theory Comput.*, 2013, **9**, 3878–3888.
- 40 A. W. Götz, M. J. Williamson, D. Xu, D. Poole, S. Le Grand and R. C. Walker, *J. Chem. Theory Comput.*, 2012, **8**, 1542–1555.
- 41 S. Le Grand, A. W. Götz and R. C. Walker, *Comput. Phys. Commun.*, 2013, **184**, 374–380.
- 42 U. Essmann, L. Perera, M. L. Berkowitz, T. Darden, H. Lee and L. G. Pedersen, *J. Chem. Phys.*, 1995, **103**, 8577–8593.
- 43 J. P. Ryckaert, G. Ciccotti and H. J. C. Berendsen, *J. Comput. Phys.*, 1977, **23**, 327–341.
- 44 J. A. Lzaguirre, D. P. Catarella, J. M. Wozniak and R. D. Skeel, *J. Chem. Phys.*, 2001, **114**, 2090–2098.
- 45 H. J. C. Berendsen, J. P. M. Postma, W. F. van Gunsteren, A. DiNola and J. R. Haak, *J. Chem. Phys.*, 1984, **81**, 3684–3690.

- 46 D. R. Roe and T. E. Cheatham, *J. Chem. Theory Comput.*, 2013, **9**, 3084–3095.
- 47 W. Humphrey, A. Dalke and K. Schulten, *J. Mol. Graph.*, 1996, **14**, 33–38.
- 48 J. Weiser, P. S. Shenkin and W. C. Still, *J. Comput. Chem.*, 1999, **20**, 217–230.